NASA Technical Memorandum 85641

NASA-TM-85641 19830018544

SOME RECENT APPLICATIONS OF XTRAN3S

DAVID A. SEIDEL, ROBERT M. BENNETT AND RODNEY H. RICKETTS

MAY 1983

NASA
National Aeronautics and
Space Administration

Langley Research Center
Hampton, Virginia 23665

SOME RECENT APPLICATIONS OF XTRAN3S

David A. Seidel, Robert M. Bennett and Rodney H. Ricketts
NASA Langley Research Center
Hampton, Virginia 23665

Abstract

A time-marching finite difference code, XTRAN3S, that solves the three-dimensional transonic small perturbation equation for flow over isolated wings has recently been developed. During initial applications of the program, problems were encountered in the prediction of unsteady forces. The use of a revised grid and force calculation scheme improved those predictions. Comparisons are made between predicted and experimental pressure data for a rectangular supercritical wing. Comparisons of steady and unsteady data at M_∞ = 0.700 show good agreement between calculated and experimental values. A comparison of steady data at M_∞ = 0.825 shows poor agreement between calculations and experiment. Program difficulties have been encountered with swept and tapered configurations.

Nomenclature

B	wing span, inches
c	nondimensional local chord, $\frac{C}{c_r}$
c_n	section normal force coefficient
c_r	reference chord, inches
C	local chord, inches
C_m	wing pitching moment coefficient
C_n	wing normal force coefficient
C_p	pressure coefficient, $\frac{p-p_\infty}{q_\infty}$
ΔC_p	lifting pressure coefficient (difference between lower and upper surface pressure coefficients)
f	oscillation frequency, Hz
F	airfoil contour
k	reduced frequency, $\frac{c_r\omega}{2V_\infty}$
$\bar{k}$	nondimensional time scaling
M_∞	freestream Mach number
p	local static pressure
p_∞	freestream static pressure
q_∞	freestream dynamic pressure
t	nondimensional time, $\frac{\bar{k}V_\infty T}{c_r}$
T	time, seconds
V_∞	freestream velocity, inches/second
x,y,z	cartesian coordinates nondimensionalized by c_r
X,Y,Z	cartesian coordinates, inches
α	angle of attack, degrees
$\Delta\alpha$	pitch oscillation amplitude, degrees
γ	ratio of specific heats
ξ,η,ζ	nondimensional transformed coordinates, (eq. 8)
$\bar{\eta}$	fractional span, $\frac{Y}{B}$
ω	frequency of oscillation, radians/second
ϕ	phase angle between pressure and wing motion, degrees (positive for pressure leading motion)
Φ	nondimensional perturbation velocity potential
Φ	velocity potential function, $\Phi = V_\infty c_r(x+\Phi)$
[ ]	denotes jump in quantity across a discontinuity

Subscripts

LE	leading edge
TE	trailing edge
o	initial or mean value

Introduction

In recent years there has been significant development of finite difference methods for solving the unsteady transonic flow equations. These methods have direct application to flutter and other aeroelastic problems which tend to be most severe in the transonic range where linearized flow analyses are inaccurate. For two-dimensional flows, methods based on the transonic small perturbation (TSP) equation are well developed. One of the most widely used programs is LTRAN2[1-2] which is used to solve the low frequency time-dependent TSP equation. The LTRAN2 code has been extended in its frequency range[3-4] and has been further extended to the complete time-dependent equation by including the Φ_{tt} term.[5] These methods have been used extensively for aeroelastic analyses (for example, see refs. 6-7 and their references).

The time-dependent solution algorithm has been extended to treat the three-dimensional TSP equation.[8-9] The resulting code, XTRAN3S, treats isolated wings and includes unsteady aerodynamic and aeroelastic analysis capability. Results are given for the low frequency equation in refs. 10 and 11 and for the full frequency equation in refs. 8, 9 and 12-15. The addition of boundary layer effects has also been demonstrated.[14]

XTRAN3S has been implemented on the CDC CYBER 203 at the NASA Langley Research Center (LaRC). This paper describes initial investigations that have been conducted to develop and validate the CYBER 203 version of the program. Results of the program are evaluated by comparison with other methods and experiment.

First, a brief review of the TSP equation and boundary conditions solved in XTRAN3S is presented. Next, assessments of and changes in the finite difference grid and the method of calculating aerodynamic forces are discussed. Calculations of steady and unsteady pressures are shown for a rectangular wing with a supercritical airfoil section that was recently tested in the Transonic Dynamics Tunnel at LaRC.[15] Comparisons of XTRAN3S predictions with the corresponding test data for a limited number of cases are presented. Program instabilities encountered for swept and tapered configurations are discussed.

XTRAN3S Program Description

The XTRAN3S program can be used to solve static and dynamic problems for rigid and elastic wings in transonic flow. A brief summary of the governing equation and boundary conditions given in refs. 9 and 10 is presented here.

A time accurate alternating direction implicit (ADI) finite difference scheme is used to solve the three-dimensional unsteady transonic small perturbation (TSP) equation

$$-(M_\infty^2\bar{k}^2\Phi_t + 2M_\infty^2\bar{k}\Phi_x)_t + (\{1-M_\infty^2\}\Phi_x + A\Phi_x^2 + B\Phi_y^2)_x + (\Phi_y + C\Phi_x\Phi_y)_y + (\Phi_z)_z = 0 \quad (1)$$

The coefficients A, B, and C depend upon the assumptions used in the development of the TSP equation. If the unsteady TSP equation is derived to be analogous to the steady, three-dimensional equation developed by Lomax et al.[16], the coefficients are defined as

$$A = -\frac{1}{2}(\gamma+1)M_\infty^2 \quad (2a)$$

$$B = \frac{1}{2}(\gamma-3)M_\infty^2 \quad (2b)$$

$$C = -(\gamma-1)M_\infty^2 \quad (2c)$$

These are referred to in ref. 10 as the "NASA/AMES" coefficients. Deriving the TSP equation from the mass conservation equation as proposed by van der Vooren et al.[17] leads to the "NLR" coefficients

$$A = -\frac{1}{2}(3-\{2-\gamma\}M_\infty^2)M_\infty^2 \quad (3a)$$

$$B = -\frac{1}{2}M_\infty^2 \quad (3b)$$

$$C = -M_\infty^2 \quad (3c)$$

The "classical" coefficients based upon an analogy to the two-dimensional steady transonic von Karman-Guderley equation are

$$A = -\frac{1}{2}(\gamma+1)M_\infty^2 \quad (4a)$$

$$B = C = 0 \quad (4b)$$

Finally, the coefficients for the linear equation are

$$A = B = C = 0 \quad (5)$$

The boundary conditions imposed upon the flow field are

Far upstream: $\Phi = 0$ (6a)

Far downstream: $\Phi_x + \bar{k}\Phi_t = 0$ (6b)

Far above and below: $\Phi_z = 0$ (6c)

Far spanwise and wing root: $\Phi_y = 0$ (6d)

Trailing vortex wake: $[\Phi_z] = 0$ (6e)

$$[\Phi_x + \bar{k}\Phi_t] = 0 \quad (6f)$$

The airfoil flow tangency condition is

$$\Phi_z^{\mp} = F_x^{\mp} + \bar{k}F_t \quad ; z = 0^{\mp},\ X_{LE} \le X \le X_{TE} \quad (7)$$

The far field boundary conditions (6c) and (6d) are equivalent to treating the computational boundaries as solid walls.

The wing is mapped into a rectangular cartesian coordinate system using the shearing transformation

$$\xi = \frac{x-x_{LE}}{c} \quad (8a)$$

$$\eta = y \quad (8b)$$

$$\zeta = z \quad (8c)$$

This maps any swept or tapered wing into a rectangular planform in the computational domain. For swept and/or tapered planforms this leads to a computational grid that is skewed in the physical domain.

The program is run at LaRC on a CDC CYBER 203 using a computational grid with 60x20x40 points in the ξ,η, and ζ directions. The CYBER 203 is capable of scalar or vector arithmetic. The scalar version of the XTRAN3S program requires 1.9 central processing unit (CPU) seconds per time step. Vectorizing the ADI ξ-sweep and a matrix manipulation routine reduces the required time to 1.2 CPU seconds per time step. Further savings in CPU time are possible by reorganizing the ADI algorithm. For a rigid rectangular wing with a 6% parabolic arc airfoil section, the solution converges to a steady state answer in 720 time steps and converges to a harmonic solution in 5 cycles (1440 time steps).

The XTRAN3S program can be used to solve for aeroelastic motions of the wing through a coupling of the aerodynamic solution and the structural equations of motion. A linear model of the structure is used and a numerical integration of the structural equations is performed for each time step in the aerodynamic calculation. The structural deformations are represented using generalized coordinates defined in terms of structural mode shapes.

XTRAN3S Program Verification

During initial applications of XTRAN3S, calculated forces exhibited spurious oscilla-

tions during convergence to a steady state solution. The cause of the oscillations was traced to the computational grid.[18] In ref. 18, an analysis of the accuracy of linear unsteady forces calculated on several two-dimensional grids was conducted. The study was carried out using a two-dimensional TSP finite difference program, XTRAN2L. Included in the grids analyzed was the default x-z grid from XTRAN3S. A revised x-z grid was described in ref. 18 which improved the accuracy of the unsteady calculations.

The first step of the program verification was to determine if accurate solutions are calculated when the code is run in a two-dimensional mode. This was done by repeating the grid study of ref. 18, using XTRAN3S with the default and revised x-z grids. Comparisons are made between calculated and theoretical values of the linear unsteady forces to determine program accuracy. The grid study was then repeated for a three-dimensional case to verify that the results of the two-dimensional analysis apply in three-dimensions.

Unsteady Force Calculation

In order to determine the accuracy of predicted forces, the linear unsteady aerodynamic forces on a flat plate were computed for a wide range of reduced frequencies. The predictions are compared to accurate solutions of the subsonic kernel function lifting-surface theory.[19-20] Unsteady forces are typically determined by calculating several cycles of forced harmonic oscillations and performing a Fourier analysis on the last cycle of oscillation. The complex fundamental component of the Fourier analysis provides the force estimate. A second approach is the indicial response method in which a Fourier transform is applied to the force response resulting from a step change in a given mode of motion. A transient pulse technique,[7,18] a variation of the indicial response method, was used to determine the unsteady forces for the present study.

In the transient pulse technique, a smoothly varying exponentially shaped pulse for a given mode of motion, (e.g. angle of attack) is applied to the wing. The unsteady calculation is carried out until all transients in the forces have decayed. A fast Fourier transform (FFT) is then applied to the input and force response time histories. The force transform is then divided by the transform of the input to obtain the unsteady aerodynamic forces for a wide range of reduced frequencies. The pulse used is described in ref. 18 and results in accurate force estimates for reduced frequencies of $k \leq 2.0$.

Two-Dimensional Analysis

Grid Effects. - The linear analysis was performed for a two-dimensional flat plate at $M_\infty = 0.850$, $\alpha_0 = 0.0^0$, $V_\infty/c_r = 50.0$ sec^{-1}, $\bar{k} = 1.0$ and $\Delta t = 0.122718$. The time step, Δt, was chosen to give a frequency increment between calculated unsteady forces of $\Delta k = 0.025$. To use XTRAN3S for linear problems, the coefficients defined in eq. (5) were used. Two-dimensional results were obtained by defining the spanwise computational grid to consist of five points, four on the wing and the fifth at the computational boundary. The two-dimensional linear results are compared to an accurate subsonic kernel function analysis.[19]

The first case analyzed is the calculation of unsteady forces using the default x-z grid described in refs. 9 and 18. A similar analysis was performed using a two-dimensional finite difference program and is detailed in ref. 18. The comparison between unsteady forces calculated using XTRAN3S and those obtained from the kernel function analysis is shown in Fig. 1. As in ref. 18, forces calculated using the default grid exhibit very poor agreement with kernel function calculations over a wide range of reduced frequencies. The oscillations exhibited in the calculated unsteady forces are due to reflections of waves that emanate from the wing. For $k < 0.3$ the oscillations are caused by reflections from the z boundary, which is treated as a solid wall (eq. 6c). For $k > 0.3$ the oscillations are caused by reflections from internal grid points due to the spacing of the computational grid in the z direction.

A revised x-z grid was proposed in ref. 18. This grid is designed to improve the calculation of unsteady forces by reducing the reflection of waves. The revised grid includes modified spacing in the z direction to minimize internal reflections, and the computational boundaries were moved further away from the wing to reduce the frequency and magnitude of the boundary reflections. The unsteady forces calculated using the revised x-z grid are shown in Fig. 2. The results obtained using the revised grid show much better agreement with those from the kernel function method for a wide range of reduced frequencies. The internal and boundary reflections have been significantly reduced, resulting in a much better comparison of forces for $k \leq 0.5$. The forces are inaccurate for $k > 0.5$ due to the continued existence of some internal reflections.

Force Calculation Techniques. For reduced frequencies in the range $0 \leq k \leq 0.5$, an offset exists between unsteady forces calculated using XTRAN3S and the kernel function method as shown in Fig. 2. The cause of this discrepancy was traced to the procedure used to calculate the forces. Forces are calculated by integrating pressures along a chord, which for the normal force coefficient is

$$c_n = \int \Delta C_p \, d\xi \tag{9}$$

In small perturbation theory the pressure coefficient is defined as

$$C_p = -\frac{2}{c}\Phi_\xi - 2\bar{k}\Phi_t \tag{10}$$

The value of Φ_ξ is computed at a grid point using linear differencing upstream and downstream of the grid point and averaging the two values. Integration of the pressures to obtain

forces is accomplished using Simpson's rule. The combination of first order differencing with second order integration can lead to an error in the force calculation.

The force calculation can be improved by integrating the potential instead of the pressures as is done in LTRAN2-NLR.[3] For the normal force coefficient, combining eqs. (9) and (10) gives

$$c_n = -\frac{2}{c}\int \Delta\Phi_\xi \delta\xi - 2\bar{k}\int \Delta\Phi_t d\xi \qquad (11)$$

where $\Delta\Phi$ is the difference between lower and upper surface potentials. The first integral can be exactly evaluated, and is equal to

$$-\frac{2}{c}(\Delta\Phi_{TE} - \Delta\Phi_{LE}) \qquad (12)$$

Since $\Delta\Phi_{LE} = 0.0$, the normal force coefficient is

$$c_n = -\frac{2}{c}\cdot\Delta\Phi_{TE} - 2\bar{k}\int \Delta\Phi_t \, d\xi \qquad (13)$$

Instead of differentiating to calculate $\Delta\Phi_\xi$ and integrating to calculate the forces, the potential jump at the airfoil trailing edge, $\Delta\Phi_{TE}$, is used in obtaining the forces.

A comparison of kernel function calculations and the unsteady forces calculated by XTRAN3S with the revised grid and alternate force calculation scheme is shown in Fig. 3. The revised force calculation has eliminated the offset in unsteady forces between XTRAN3S and kernel function calculations. For a flat plate, the forces show very good agreement for reduced frequencies up to k = 0.6.

Three-Dimensional Analysis

The linear analysis was performed for a flat plate rectangular wing at $M_\infty = 0.850$, $\alpha_0 = 0.0^0$, $V_\infty/c_r = 50.0$ sec^{-1}, $\bar{k} = 1.0$ and $\Delta t = 0.122718$. The rectangular wing has a panel aspect ratio of 3.30. As in the two-dimensional analysis, the coefficients defined in eq. (5) were used. The spanwise computational grid is the same as that described in ref. 9, consisting of 15 equi-spaced points on the wing with an additional point defining the wing tip and 4 grid points outboard of the wing. The three-dimensional XTRAN3S results are compared to an accurate calculation using the three-dimensional subsonic kernel function.[20]

Unsteady forces were calculated using the default x-z grid on the rectangular flat plate using the revised force calculation method. Comparison between the calculated unsteady force and kernel function predictions is shown in Fig. 4. As in the two-dimensional case, forces calculated using the XTRAN3S default x-z grid exhibit very poor agreement with kernel function calculations. The kernel function results for k > 1.5 are erratic due to a program limit in the numerical quadrature used.

Using the revised x-z grid with the same y grid as above leads to the results shown in Fig. 5. The XTRAN3S calculated forces agree well with the kernel function forces for $0.2 \lesssim k \lesssim 0.6$. The cause of the low frequency discrepancy is unknown, but the cause of the discrepancy at high frequencies is the same as in the two-dimensional analysis - reflections of disturbances within the computational domain. The analysis was performed using several spanwise grid spacings, and the calculations were found to be only slightly influenced by the spanwise spacing.

Comparisons With Experiment

In this section, comparisons of XTRAN3S calculations and experimental data obtained from a rectangular wing recently tested in the Langley Transonic Dynamics Tunnel[15] are presented. The wing has a panel aspect ratio of 2.0 and a 12% thick supercritical airfoil section. Pressure measurements were made at four spanwise stations over a broad range of Mach number and angle of attack for both static pitch and oscillations in pitch about 0.46 chord. The test Reynolds number was 4.0 million based on chord and the test medium was Freon ($\gamma = 1.131$). Further description of the tests and the model are given in ref. 15. All calculations were made using measured airfoil ordinates and for measured root angle of attack and Mach number. The revised x-z grid was used for all subsequent calculations.

Steady Results

The steady state calculations are compared with measured data for $\alpha_0 = 2.0^0$ and for $M_\infty = 0.700$ and 0.825 in Figs. 6 and 7 respectively. Calculations were made using the AMES (eq. 2) and NLR (eq. 3) coefficients in the TSP equation. For $M_\infty = 0.700$ (Fig. 6) there is a weak shock near the inboard leading edge. The agreement with the data is generally good over the mid portion of the chord but with some deviation near the nose and the lower trailing edge regions. There is little difference in the results obtained using the NLR or the AMES coefficients except near the shock. The NLR coefficients give a somewhat stronger shock for this case. Some of the lack of agreement in the nose area may be a result of using a relatively coarse grid near the nose.

For $M_\infty = 0.825$ (Fig. 7), the shock is further aft on the inboard portion of the wing and approaches the leading edge at the tip, showing a large three-dimensional effect. The correlation of the computed results with the experimental data shows trends similar to the results for $M_\infty = 0.700$, but with signficantly poorer agreement. The NLR coefficients give a shock that is significantly stronger and located further aft than that predicted using the AMES coefficients.

A sample two-dimensional calculation has been made for this airfoil using a non-conservative full potential program[21] with

and without a boundary layer. The results for $M_\infty = 0.825$ and $\alpha_0 = 0^0$ are shown in Fig. 8. There is a qualitative correspondence of the trend shown with and without a boundary layer (Fig. 8) to the correlation between the inviscid XTRAN3S calculations and the measured data at $M_\infty = 0.825$ (Fig. 7). This suggests that viscous effects are significant for this supercritical wing. The boundary layer addition to XTRAN3S[14] has not yet been implemented at Langley. It would appear that further effort in viscous calculations is necessary.

It appears that better correlation between the inviscid full potential (Fig. 8) and XTRAN3S calculations (Fig. 7) is obtained when the NLR coefficients are used. At the inboard span station, the results from XTRAN3S with the NLR coefficients show a shock at the trailing edge, which agrees with the two-dimensional full potential prediction.

Unsteady Results

Due to the poor agreement in steady state pressures betwen experiment and XTRAN3S calculations at $M_\infty = 0.825$, unsteady data comparisons between experiment and calculations are shown only for $M_\infty = 0.700$. At this Mach number the best comparison of steady state pressures between experiment and XTRAN3S calculations is obtained using the NLR coefficients (see Fig. 6). Using the NLR coefficients gives a stronger shock on the inboard region of the wing, which comes closer to matching the experimental data. Based on this observation, the NLR coefficients were used for all unsteady analysis at $M_\infty = 0.700$.

Unsteady results for $M_\infty = 0.700$, $\alpha_0 = 2.0^0$, $\Delta\alpha = \mp 1^0$, $k = 0.178$ and $f = 10$ Hz are shown in Fig. 9 in the form of magnitude and phase of the lifting pressure coefficient. Corresponding results are shown from XTRAN3S using the NLR coefficients and from linear lifting surface theory (RHOIV)[22]. The pressure amplitudes calculated by XTRAN3S are in good agreement with the experimental data over most of the wing with some over prediction in the inboard leading edge region and under prediction over the outboard portion of the wing. The linear theory results are in good agreement with experiment except near the leading edge where transonic effects are evident. As for the pressure amplitude, the XTRAN3S results for phase show an over prediction in the inboard leading edge region. An examination of the experimental data reveals that the large change in the phase data occurs over the trailing edge portion of the wing's lower surface and is probably caused by viscous effects. The linear theory results for phase are in good agreement with experiment over the forward part of the airfoil. The best agreement between XTRAN3S calculations and experimental data occurs in the mid-span region where the dynamic shock is not over predicted and tip effects are not pronounced.

Similar results are shown in Fig. 10 for $k = 0.356$ and $f = 20$ Hz. The comparison with XTRAN3S is improved for this higher reduced frequency, particularly in the phase near the trailing edge. The linear theory pressure amplitude prediction is not as good as that for $f = 10$ Hz, under predicting the pressure near the leading edge and over predicting the pressure near the trailing edge.

Numerical Stability

As previously discussed, an ADI scheme is used in XTRAN3S. For rectangular wings the program exhibits good numerical stability, becoming unstable only for large Δt. Several attempts to analyze wings with moderate sweep and taper have been unsuccessful due to a numerical instability which appears to be independent of Δt. The instability has been encountered for wings with taper ratios of approximately 0.3 and leading edge sweep from 29^0-36^0. Planforms for which the instability has been encountered include those of the F-5, AV-8B and DAST ARW-2 wings. Successful calculations have been made for the LANN wing[13] which has a taper ratio of 0.4 and leading edge sweep of 27.5^0. Thus only wings of low to medium sweep and taper have been successfully treated.

The source of the instability is not clear at this time. It may be related to the highly skewed physical computational grid which results from the shearing transformation (eq. 8a) or to how some of the terms are treated in the finite difference scheme. For a wing with moderate sweep and taper, a typical x-y plane of the grid in physical coordinates is shown in Fig. 11. The grid is highly skewed in the upstream and downstream regions, and the grid points are closely spaced outboard of the wing. This can possibly lead to computational difficulties. The problem is currently being addressed, but until it is resolved program applications are limited to wings of low sweep and taper.

Concluding Remarks

A comparison of unsteady forces calculated using the XTRAN3S program and accurate theoretical methods for a flat plate airfoil demonstrated inaccuracies in the forces predicted by XTRAN3S. The cause was found to be the reflection of waves from the computational boundaries and internal grid points. A new grid significantly reduced errors caused by these reflections. A revised scheme for calculating unsteady forces improved the agreement of calculated and accurate kernel function values. A comparison of calculated unsteady forces and those predicted by a kernel function method for a flat plate rectangular wing demonstrated good agreement using the revised grid and force calculation scheme.

Comparison of calculations for a rectangular supercritical wing with wind tunnel data showed mixed agreement. Comparisons of steady and unsteady pressures for $M_\infty = 0.700$ showed good agreement while comparisons of steady pressures for $M_\infty = 0.825$ showed poor agreement. Steady state calculations at $M_\infty = 0.825$ showed a large effect of the equation coefficients used.

Comparing the experimental data with calculations pointed out the need for viscous effects in an XTRAN3S-type code.

Experience with of other configurations using the XTRAN3S program demonstrated a numerical instability. The instability occurred for wings with moderate sweep and taper. Further improvements are needed to extend the applicability of the program to these cases.

References

[1]Ballhaus, W. F. and Goorjian, P.M.: Implicit Finite-Difference Computations of Unsteady Transonic Flow About Airfoils. AIAA Journal, vol. 15, no. 12, Dec. 1977, pp. 1728-1735.

[2]Ballhaus, W. F., and Goorjian, P. M.: Computation of Unsteady Transonic Flows by the Indicial Method. AIAA Journal, vol. 16, no. 2, Feb. 1978, pp. 117-124.

[3]Houwink, R., and van der Vooren, J.: Improved Version of LTRAN2 for Unsteady Transonic Flow Computations. AIAA Journal, vol. 18, no. 8, Aug. 1980, pp. 1008-1010.

[4]Hessenius, K. A. and Goorjian, P. M.: Validation of LTRAN2-HI by Comparison with Unsteady Transonic Experiment. AIAA Journal, vol. 20, no. 5, May 1982, pp. 731-732.

[5]Rizzetta, D. P., and Chin, W. C.: Effect of Frequency in Unsteady Transonic Flow. AIAA Journal, vol. 17, no. 7, July 1979, pp. 779-781.

[6]Edwards, J. W., Bennett, R. M., Whitlow, W., Jr., and Seidel, D. A.: Time-Marching Transonic Flutter Solutions Including Angle-of-Attack Effects. AIAA Paper 82-0685, May 1982.

[7]Bland, S. R., and Edwards, J. W.: Airfoil Shape and Thickness Effects on Transonic Airloads and Flutter. AIAA Paper No. 83-0959, May 1983.

[8]Borland, C. J., and Rizzetta, D. P.: Transonic Unsteady Aerodynamics for Aeroelastic Applications - Vol. I: Technical Development Summary. AFWAL TR 80-3107, Vol. I, June 1982.

[9]Borland, C. J., and Rizzetta, D. P.: Nonlinear Transonic Flutter Analysis. AIAA Journal, vol. 20, no. 11, Nov. 1982, pp. 1606-1615.

[10]Borland, C. J., Rizzetta, D. P., and Yoshihara, H.: Numerical Solution of Three-Dimensional Unsteady Transonic Flow Over Swept Wings. AIAA Journal, vol. 20, no. 3, March 1982, pp. 340-347.

[11]Guruswamy, P., and Goorjian, P.M.: Comparisons Between Computations and Experimental Data In Unsteady Three-Dimensional Transonic Aerodynamics, Including Aeroelastic Applications. AIAA Paper 82-0690, May 1982.

[12]Myers, M. R., Guruswamy, P., and Goorjian, P. M.: Flutter Analysis for a Transport Wing Using XTRAN3S. AIAA Paper 83-0922, May 1983.

[13]Ruo, S. Y., Malone, J. B., Horsten, J. J., and Houwink, R.: LANN Program: An Experimental and Theoretical Study of Steady and Unsteady Transonic Airloads on a Supercritical Wing. AIAA Paper 83-1686, July 1983.

[14]Rizzetta, D. P., and Borland, C. J.: Unsteady Transonic Flow over Wings Including Inviscid/Viscous Interactions. AIAA Journal vol. 21, no. 3, March 1983, pp. 363-371.

[15]Ricketts, R. R. Sandford, M. S., Seidel, D. A., and Watson, J. J.: Transonic Pressure Distributions On a Rectangular Supercritical Wing Oscillating in Pitch. AIAA Paper 83-0923, May 1983.

[16]Lomax, H., Bailey, F. R., and Ballhaus, W. F.: On the Numerical Simulation of Three-Dimensional Transonic Flow with Application to the C-141 Wing. NASA TN D-6933, August 1973.

[17]van der Vooren, J., Sloof, J. W., Huizing, G. H., and van Essen, A.: Remarks on the Suitability of Various Transonic Small Perturbation Equations to Describe Three-Dimensional Transonic Flow; Examples of Computations Using a Fully-Conservative Rotated Difference Scheme. Symposium Transsonicum II, Gottingen, West Germany, September 1975, proceedings, Springer-Verlag, Berlin, 1976, pp. 557-566.

[18]Seidel, D. A., Bennett, R. M., and Whitlow, W., Jr.: An Exploratory Study of Finite Difference Grids for Transonic Unsteady Aerodynamics. AIAA Paper 83-0503, January 1983.

[19]Bland, S. R.: Development of Low-Frequency Kernel-Function Aerodynamics for Comparison with Time-Dependent Finite-Difference Methods. NASA TM 83283, May 1982.

[20]Desmarais, R. N. and Bennett, R. M.: User's Guide for a Modular Flutter Analysis Software System (FAST Version 1.0). NASA TM 78720, May 1978.

[21]Bauer, F., Garabedian, P., Korn, D., and Jameson, A.: Supercritical Wing Section II. Lecture Notes in Economics and Mathematical Systems. M. Beckmann and H. R. Lunzi, eds. Springer-Verlag, 1975.

[22]Redman, M. C., and Rowe, W. S.: Prediction of Unsteady Aerodynamic Loadings Caused by Leading Edge and Trailing Edge Control Surface Motions in Subsonic Compressible Flow -- Computer Program Description. NASA CR 132634, May 1975.

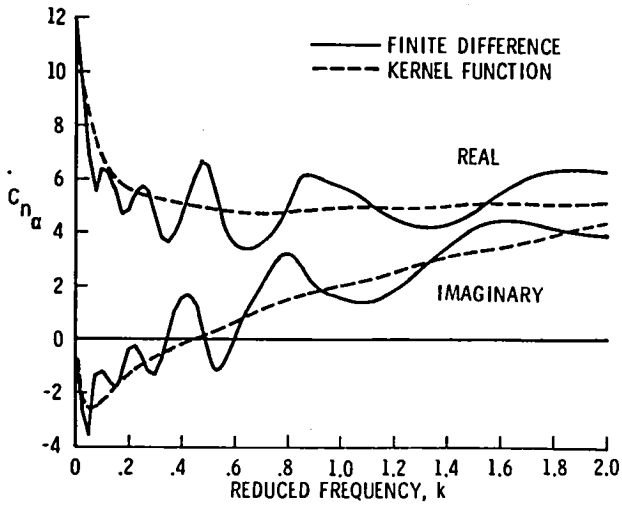

Fig. 1 - Unsteady forces calculated for a flat plate airfoil using default XTRAN3S x-z grid, M_∞ = .850.

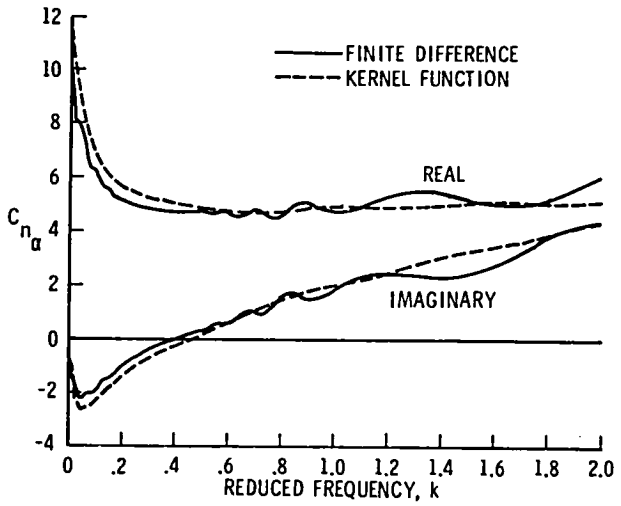

Fig. 2 - Unsteady forces calculated for a flat plate airfoil using revised XTRAN3S x-z grid, M_∞ = .850.

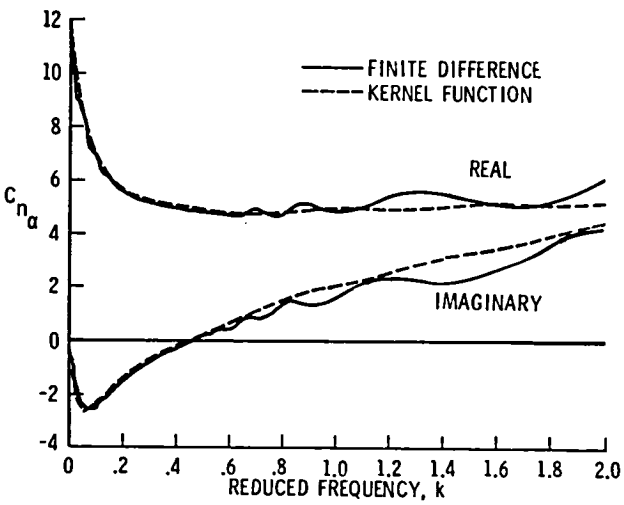

Fig. 3 - Unsteady forces calculated for a flat plate airfoil using revised XTRAN3S x-z grid and revised force calculation scheme, M_∞ = .850.

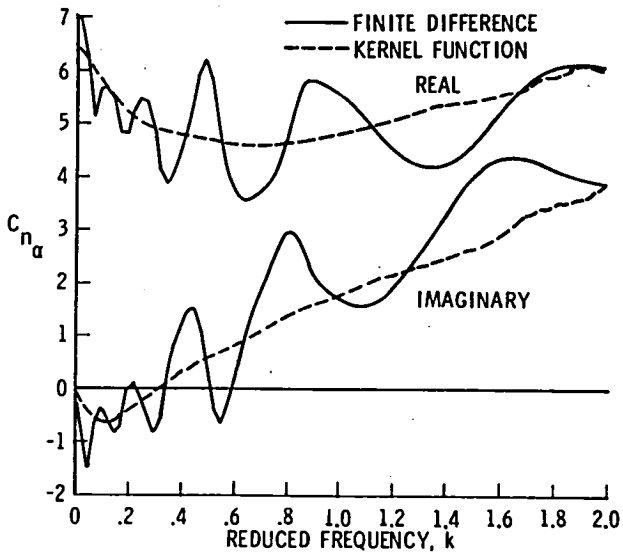

Fig. 4 - Unsteady forces calculated for a flat plate rectangular wing using default XTRAN3S grid, M_∞ = .850.

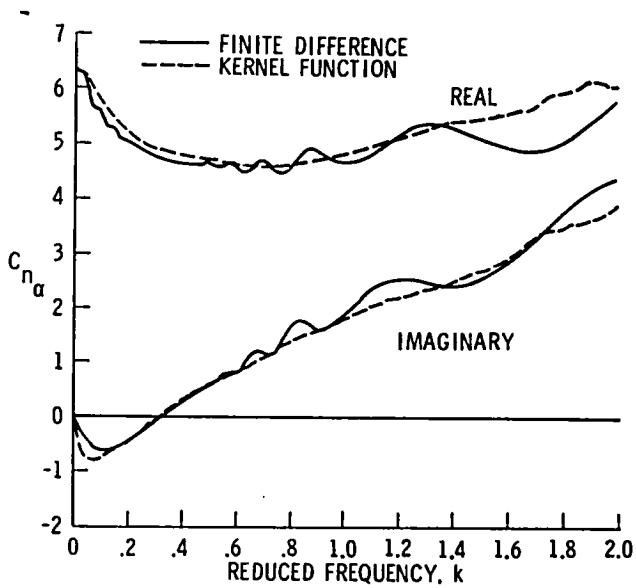

Fig. 5 - Unsteady forces calculated for a flat plate rectangular wing using revised XTRAN3S grid, M_∞ = .850.

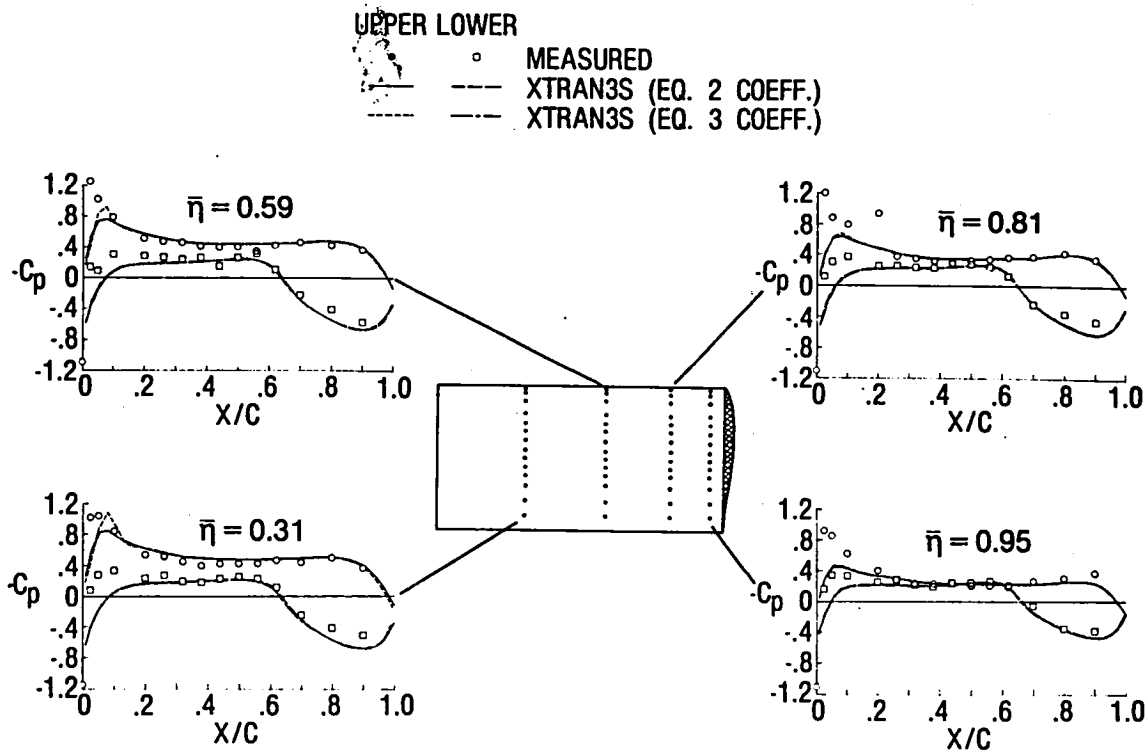

Fig. 6 - Comparison of measured and calculated steady state pressure distributions for rectangular supercritical wing, $M_\infty = 0.700$, $\alpha_0 = 2^o$.

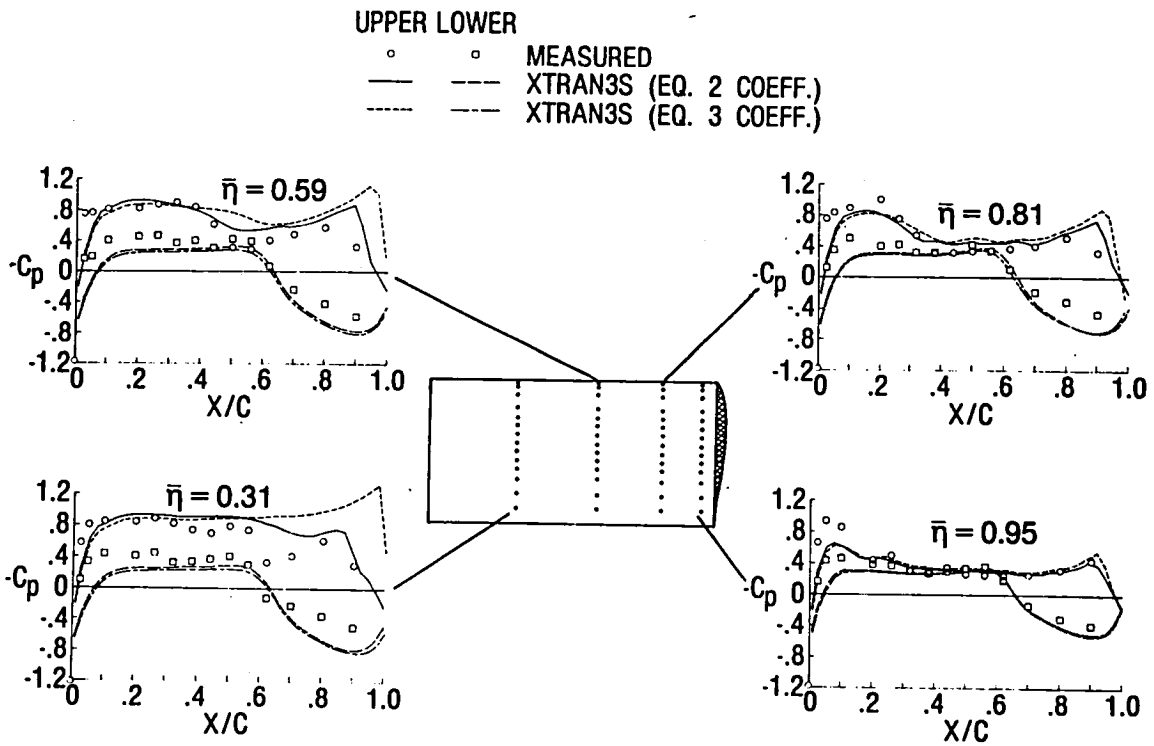

Fig. 7 - Comparison of measured and calculated steady state pressure distributions for rectangular supercritical wing, $M_\infty = 0.825$, $\alpha_0 = 2^o$.

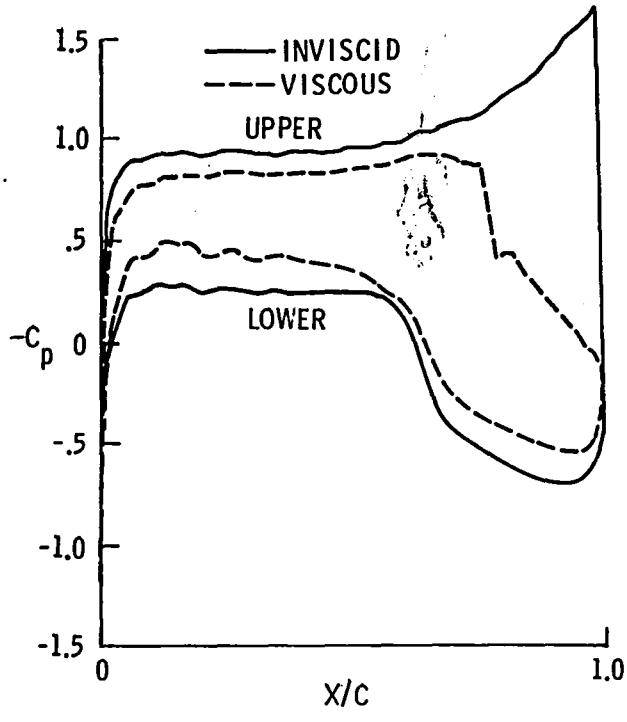

Fig. 8 - Comparison of inviscid and viscous full potential calculations of steady state pressure distribution for supercritical airfoil, $M_\infty = 0.825$, $\alpha_0 = 0^o$.

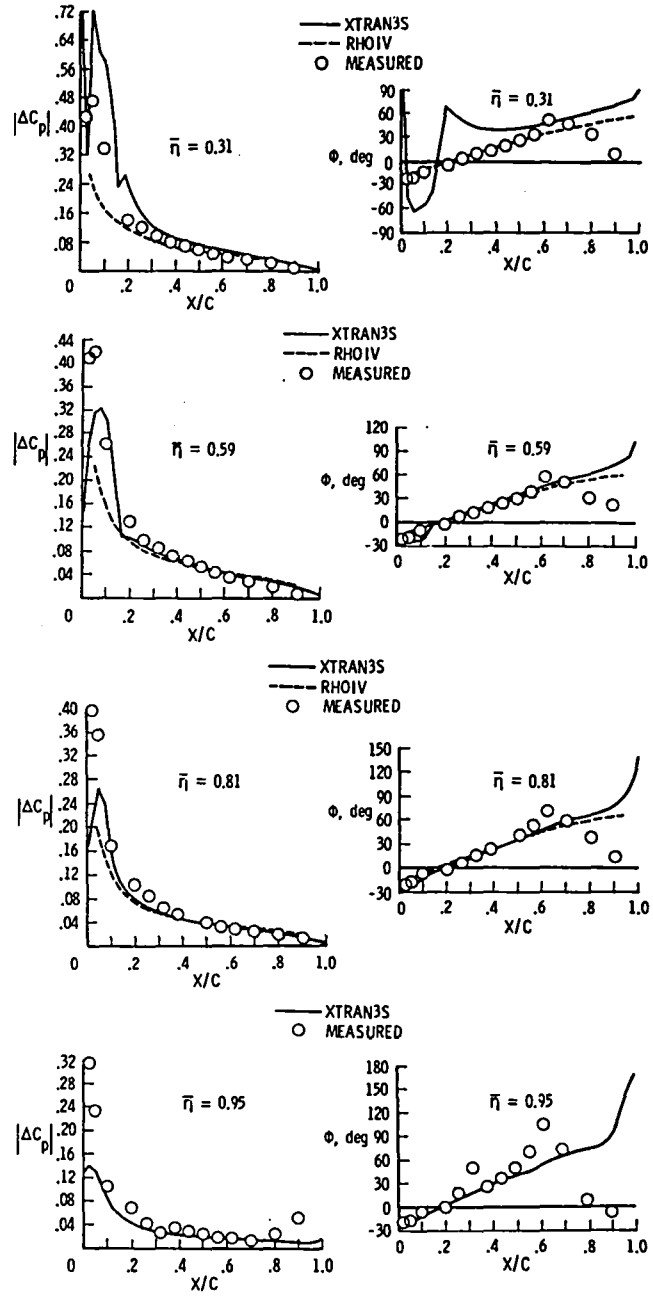

Fig. 9 - Comparison of measured and calculated unsteady pressures for rectangular supercritical wing, $M_\infty = 0.700$, $\alpha_0 = 2^o$, $\Delta\alpha = \mp 1^o$, $k = 0.178$ (Ref. 15, Fig. 14).

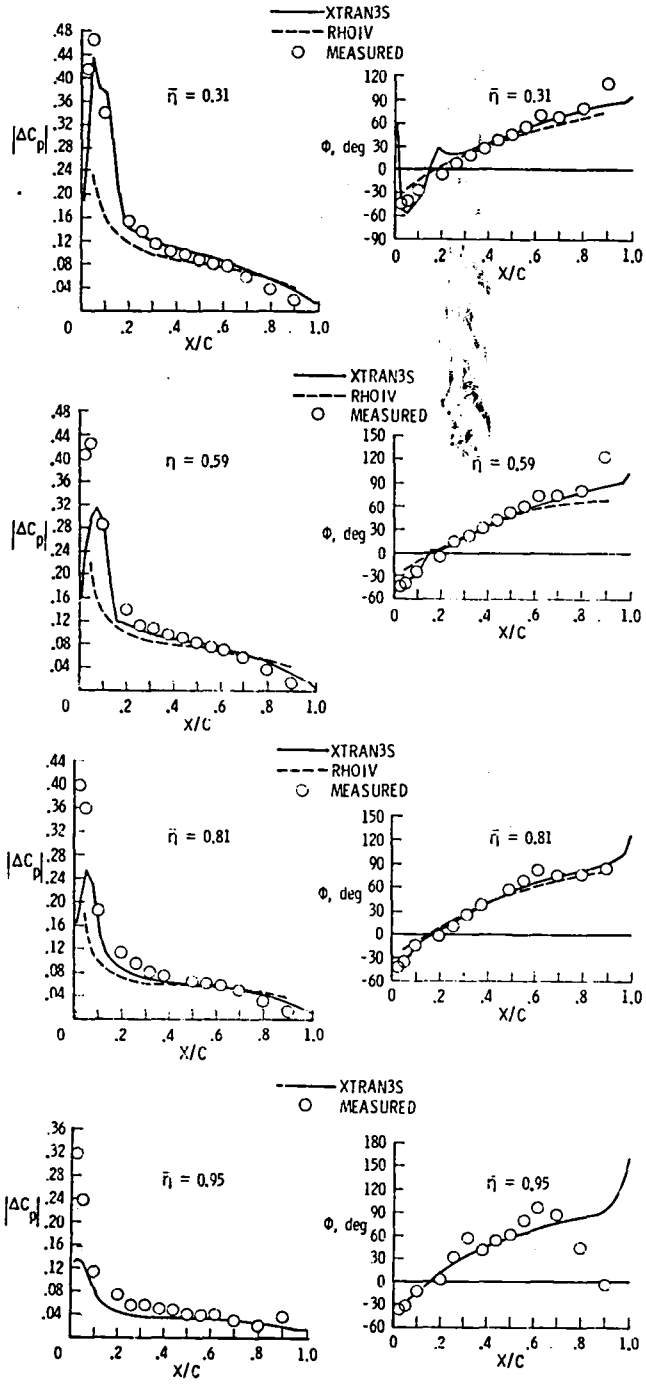

Fig. 10 - Comparison of measured and calculated unsteady pressures for rectangular supercritical wing, $M_\infty = 0.700$, $\alpha_0 = 2^0$, $\Delta\alpha = \mp 1^0$, $k = 0.356$.

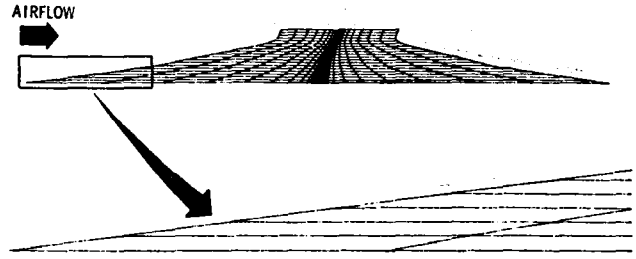

Fig. 11 - Typical x-y plane of computational grid for wing with moderate sweep and taper.

1. Report No.	2. Government Accession No.	3. Recipient's Catalog No.
NASA TM-85641		

4. Title and Subtitle	5. Report Date
Some Recent Applications of XTRAN3S	May 1983
	6. Performing Organization Code 505-33-43-09

7. Author(s)	8. Performing Organization Report No.
David A. Seidel, Robert M. Bennett and Rodney H. Ricketts	
	10. Work Unit No.
9. Performing Organization Name and Address	
NASA Langley Research Center Hampton, VA 23665	11. Contract or Grant No.
	13. Type of Report and Period Covered
12. Sponsoring Agency Name and Address	Technical Memorandum
National Aeronautics and Space Administration Washington DC 20546	14. Sponsoring Agency Code

15. Supplementary Notes

Presented as AIAA Paper No. 83-1811 at the AIAA Applied Aerodynamics Conference, Danvers, MA, July 13-15, 1983

16. Abstract

A time-marching finite difference code, XTRAN3S that solves the three-dimensional transonic small perturbation equation for flow over isolated wings has recently been developed. During initial applications of the program, problems were encountered in the prediction of unsteady forces. The use of a revised grid and force calculation scheme improved those predictions. Comparisons are made between predicted and experimental pressure data for a rectangular supercritical wing. Comparisons of steady and unsteady data at $M_\infty = 0.700$ show good agreement between calculated and experimental values. A comparison of steady data at $M_\infty = 0.825$ shows poor agreement between calculations and experiment. Program difficulties have been encountered with swept and tapered configurations.

17. Key Words (Suggested by Author(s))	18. Distribution Statement
Finite Difference Transonic Small Perturbation Equation Grids Unsteady Aerodynamics	Unclassified - Unlimited Subject Category 02

19. Security Classif. (of this report)	20. Security Classif. (of this page)	21. No. of Pages	22. Price
Unclassified	Unclassified	11	A02

For sale by the National Technical Information Service, Springfield, Virginia 22161